



ELSEVIER

Available online at www.sciencedirect.com

SCIENCE @ DIRECT®

Computers and Mathematics with Applications 49 (2005) 1355–1373

An International Journal
**computers &
mathematics**
with applications

www.elsevier.com/locate/camwa

The Optimal Centroidal Voronoi Tessellations and the Gersho's Conjecture in the Three-Dimensional Space

QIANG DU

Department of Mathematics
Penn State University, PA 16802, U.S.A.
qdu@math.psu.edu

and

Academy of Mathematics and Systems Science
Chinese Academy of Sciences, Beijing 100080, P.R. China

DESHENG WANG

Department of Mathematics, University of Xiangtan
Hunan 411105, P.R. China

and

Civil and Computational Engineering Centre
School of Engineering, University of Wales Swansea
Singleton Park, Swansea SA2 8PP, U.K.
desheng.wang@swansea.ac.uk

(Received August 2004; revised and accepted December 2004)

Abstract—Optimal centroidal Voronoi tessellations have important applications in many different areas such as vector quantization, data and image processing, clustering analysis, and resource management. In the three-dimensional Euclidean space, they are also useful to the mesh generation and optimization. In this paper, we conduct extensive numerical simulations to investigate the asymptotic structures of optimal centroidal Voronoi tessellations for a given domain. Such a problem is intimately related to the famous Gersho's conjecture, for which a full proof is still not available. We provide abundant evidence to substantiate the claim of the conjecture: the body-centered-cubic lattice (or Par6) based centroidal Voronoi tessellation has the lowest cost (or energy) per unit volume and is the most likely congruent cell predicted by the three-dimensional Gersho conjecture. More importantly, we probe the various properties of this optimal configuration including its dual triangulations which bear significant consequences in applications to three-dimensional high quality meshing.
© 2005 Elsevier Ltd. All rights reserved.

Keywords—Optimal triangulation, Centroidal Voronoi Tessellation, Gersho's conjecture, Optimal vector quantizer, Mesh generation and optimization.

We would like to thank the referee for many helpful suggestions that improved our presentation. The research was supported in part by the China State Major Basic Research Fund G199903280 and by the NSF-DMS 0196522.

0898-1221/05/\$ - see front matter © 2005 Elsevier Ltd. All rights reserved.
doi:10.1016/j.camwa.2004.12.008

Typeset by $\mathcal{A}\mathcal{M}\mathcal{S}\text{-T}\mathcal{E}\mathcal{X}$

1. INTRODUCTION

A centroidal Voronoi tessellation (CVT) is a Voronoi tessellation of a region such that the generating points of the tessellations are also the mass centroids of the corresponding Voronoi regions with respect to a given density function [1]. Its dual triangulation is called the centroidal Voronoi Delaunay triangulation (CVDT) [2,3]. CVTs enjoy an optimization characterization so that they turn out to be useful in diverse applications such as image and data analysis, vector quantization, resource optimization, optimal placement of sensors and actuators for control, cell biology, territorial behavior of animals, high quality mesh generation, numerical partial differential equations, meshless computing, etc., [1,3–7]. Given a domain, a specific density and a fixed number of generators, the optimal CVT is defined as one which has the lowest cost functional (or energy, distortion) among all the possible CVTs. Such configurations are directly related to the celebrated Gershgorin conjecture. The conjecture was originally stated for optimal vector quantizers used in data compression and transmission [8], and translating in the language of CVTs [1], it states that *asymptotically as the number of generators gets larger and larger, the optimal CVT will be forming a regular tessellation consisting of the replication of a single polytope whose shape depends only on the spatial dimension*. The basic Voronoi cell of the optimal CVT was shown to be the regular hexagon in two dimensions [9]. For the three-dimensional space with a constant density function, it was proved that among all lattice-based CVTs, the CVT corresponding to the body-centered cubic lattice (BCC) is the optimal one [10]; while for nonlattice cases or the general cases, the conclusion remains to be rigorously proved [8,11].

In this paper, we conduct some well-organized numerical experiments on CVTs to provide a clear substantiation of the Gershgorin conjecture in 3D: the BCC lattice based CVT is not only optimal among the lattice based ones, but also is likely the global optimal solution for all the CVTs including nonlattice ones. The computations are done mostly via the classical Lloyd iterations [12]. While the convergence of such iterations to a CVT configuration is mostly assured [13], its convergence to the global optimum is dependent on the choice of the initial configuration. We demonstrate that the optimal CVT and its dual CVDT enjoy very nice geometrical and topological properties, and they lead to high quality tetrahedral meshes in the three-dimensional space. For simplicity, much of our simulations are carried out for the constant density case since we are mostly interested in establishing results in the asymptotic regime where the variation of the density in space is less important. Such a simplification also allows us to conduct numerical experiments on relatively smaller scales than those otherwise required for more complicated nonuniform densities. In addition, we also design careful experiments in various geometry to address the boundary effect on the simulation results.

The remainder of the paper is organized as follows: first in Section 2, we discuss how to compute the optimal CVTs, mostly based on the Lloyd iterations. In Section 3, abundant examples are presented to show that the BCC based CVT is likely the optimal CVT for both lattice and nonlattice based configurations. In Section 4, we illustrate the dependence on the initial configurations of the Lloyd iterations and we also address the boundary effects. In Section 5, the qualities of the converged three-dimensional CVT and CVDT are discussed and we give hints on the possible application to high quality meshing. Finally, some conclusions are drawn in Section 6.

2. BASICS OF THE CVT AND THE LLOYD ITERATION

Given a set of input points $\{z_i\}_1^n$ belonging to a domain $\Omega \subset R^k$, the Voronoi region \hat{V}_i corresponding to the point z_i consists of all points in Ω that are closer to z_i than to any other point in the set. The set $\{\hat{V}_i\}_1^n$ forms a partition of Ω and is known as a *Voronoi tessellation* or *Voronoi diagram* of Ω . The points $\{z_i\}_1^n$ are called *generating points* or *generators*. The dual *Delaunay triangulation* is formed by connecting pairs of generating points which correspond to adjacent Voronoi regions [14,15].

Given a density function ρ defined on any region V_i , the *mass centroids* \mathbf{z}_i^* of V_i is defined by

$$\mathbf{z}_i^* = \frac{\int_{V_i} \mathbf{y} \rho(\mathbf{y}) d\mathbf{y}}{\int_{V_i} \rho(\mathbf{y}) d\mathbf{y}}.$$

A Voronoi tessellation is a *centroidal Voronoi tessellation* (CVT) if $\mathbf{z}_i = \mathbf{z}_i^*$, for all i , i.e., the generators of the Voronoi regions are themselves the mass centroids of those regions. The dual Delaunay triangulation of CVT is referred to as the *centroidal Voronoi-Delaunay triangulation* (CVDT). When geometric constraints are present, such as the constraints on the boundary vertices, the corresponding definitions of the CVT and CVDT may be generalized to the constrained CVT and constrained CVDT [3,16] and anisotropic CVTs [17].

2.1. Lloyd Iteration for Constrained Centroidal Voronoi Tessellation

There are several algorithms known for constructing centroidal Voronoi tessellation of a given set [1,18], and they can be categorized into two approaches: the probabilistic and the deterministic approaches. A representative of the probabilistic algorithms is the method by MacQueen using an elegant random sequential sampling and averaging technique [19]. Faster acceleration of the MacQueen’s method and its parallel implementation are given in [18]. The deterministic Lloyd algorithm is the obvious iteration between computing Voronoi diagrams and mass centroids [12]. In quantization and clustering literature, one can also find the related h -means and k -means algorithms for the construction of discrete CVTs [11,20]. Here, we choose to work with the Lloyd’s method for the construction of three-dimensional CVT and its dual triangulation CVDT mostly because of interests in the energy minimum and the fact that the Lloyd iteration enjoys the energy decreasing property [1].

Given a three-dimensional bounded domain and a sizing function, to construct a constrained three-dimensional CVT (with the generators on the boundary being fixed), the original Lloyd iteration is efficiently implemented through the following procedure [3].

- 0 Construct an initial conforming or constrained Delaunay tetrahedronization of a given 3D domain (upon the input of a surface triangular mesh) under a given sizing field $H(p)$ for any given point p in the domain [3]. Here, $H(p)$ can be prespecified or derived from the sizing of the boundary points. Let all the data of the conforming/constrained boundary tetrahedronization be stored.
- 1 Construct the Voronoi regions for all interior points that are allowed to change their positions, and construct the mass centers of the Voronoi regions with a properly defined density function ρ derived from the sizing field $H(p)$. Here, the Voronoi regions can be computed directly from the Delaunay tetrahedronization via the duality relationship.
- 2 Insert the computed mass centers into the conforming boundary tetrahedronization via the constrained Delaunay insertion procedure [3].
- 3 Compute the difference $D = \sum_{i=1}^n \|P_i - P_{imc}\|^2$, where $\{P_i\}$ is the set of interior points allowed to change, and $\{P_{imc}\}$ is the the set of corresponding computed mass center.
- 4 If D is less than a given tolerance, terminate; otherwise, return to Step 1.

In [3], the Lloyd iteration was used for the tetrahedral mesh generation and optimization. Here, it is applied to construct numerous three-dimensional CVTs and their dual CVDTs in order to substantiate the three-dimensional Gersho’s conjecture.

2.2. Energy (or Cost) Per Unit Volume and Optimal CVTs

Given a density function ρ , a tessellation $V = \{V_i\}_1^n$ of the domain Ω and a set of points $Z = \{z_i\}_1^n$ in Ω , we can define the following cost functional:

$$\mathcal{F}(V, Z) = \sum_{i=1}^n F(V_i, z_i), \quad \text{where } F(V_i, z_i) = \int_{V_i} \rho(x) \|x - z_i\|^2 dx. \tag{1}$$

This cost functional is also called by other names such as the energy, the error, and the distortion value depending on the type of applications in mind [1]. The standard CVTs along with their generators are critical points of this cost functional (1), as shown in [1]. The Lloyd iteration described earlier enjoys the property that the related functional or cost is monotonically decreasing throughout the iteration [1] thus providing a possible clue for its convergence. More theoretical analysis on the convergence properties of the Lloyd iteration has recently been made in [13].

The *energy (or cost) per unit volume* (E_p) for a partition or tessellation $\{V, Z\}$ is then defined by:

$$D(V, Z) = \frac{n^{2/k} \mathcal{F}(V, Z)}{k |\Omega|^{1+2/k}}.$$

Here, k is the dimension of the space ($k = 3$ in our paper), $|\Omega|$ the volume of $\Omega = \bigcup_{i=1}^n V_i$.

For a given bounded domain Ω together with a specified density function and a fixed number of generator, an *optimal CVT* is defined as a global minimum of $\mathcal{F}(V, Z)$, while the optimal centroidal Voronoi tessellation in a given Euclidean-dimensional space (e.g., the two-dimensional space), asymptotically speaking, is defined as the CVT which has the lowest energy per unit volume among all CVTs that cover the whole space (as the number of generators going to infinity).

The optimal CVT concept is closely related to the *Gershho's conjecture* [8], which states that: *asymptotically speaking, all cells of the optimal CVT, while forming a tessellation, are congruent to a basic cell which depends on the dimension.* This claim is trivially true in one dimension. It has been proved for the two-dimensional case [9] with the basic cell being the two-dimensional regular hexagon. Gershho's conjecture remains open for three and higher dimensions [11]. In [10], it was shown that the body-centered-cubic (BCC) lattice based CVT enjoys the lowest energy per unit volume among all possible lattice based CVTs. The BCC based CVTs has the energy per unit volume valued at 0.07854, with the basic cell given by the truncated octahedron. Other lattices, such as FCC, A15, and Z have the energy values 0.07874, 0.08098 and 0.08666 respectively. Some basic Voronoi cells for the lattice based CVTs are given in Figure 1.

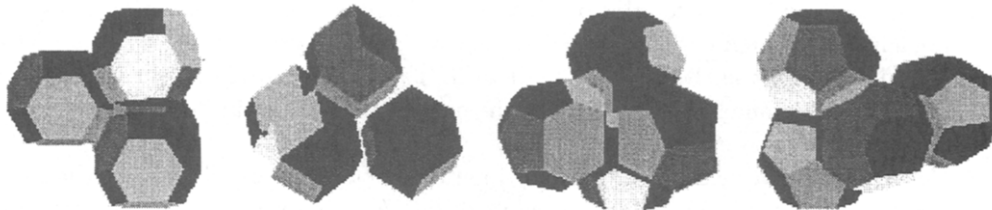


Figure 1. Basic Voronoi cells of the BCC, FCC, A15, and Z configurations.

In [21], variants of A15 were also studied, but they were shown to be inferior to the BCC based CVTs. For nonlattice based or general CVTs, it remains unresolved whether the BCC enjoys the lowest energy per unit volume [11]. One question pertains to the possibility of having the optimal CVT made up by a combination of several types of basic cells. In later sections, we design a series of numerical examples for both lattice and nonlattice based CVTs. The computed energy per unit volume and other related properties and statistics substantiate the claim of the three-dimensional Gershho's conjecture: *the BCC based CVT enjoys the lowest energy among all three-dimensional CVTs including both lattice and nonlattice CVTs.* Thus, asymptotically speaking, the congruent cell of the optimal CVT is the Voronoi cell of the BCC based tessellation, that is, the truncated octahedron.

3. NUMERICAL SUBSTANTIATION OF THE 3D GERSHO CONJECTURE

To provide convincing numerical evidence for the Gershho conjecture beyond the lattice based argument, in this section, three-dimensional constrained centroidal Voronoi tessellations are con-

structured via the Lloyd iteration for general nonlattice settings. The experiments are designed based on the rationale that, on one hand, the Lloyd iteration always converges to a CVT in practice for any geometry [12,13], and on the other hand, a clear understanding is needed concerning the effect of the geometry boundary, the distribution of initial points and the mesh topological configuration on the final outcome of the Lloyd iteration. Accordingly, this calls for the use of different initial arrangements in planning our numerical experiments so that we may examine the structure of the converged CVT, and determine whether the result tends to the expected pattern.

For a given domain, the initial input of the Lloyd iteration includes a surface triangulation and a distribution of initial field or interior points. The vertices of the surface triangulation and the interior points together make up all the generators of the Voronoi tessellation. Depending on the input geometry and the initial conditions, the optimal CVTs to be computed can be classified into roughly two categories: lattice based CVTs and nonlattice based or general unstructured CVTs. In the former category, all the initial surface triangulations and the interior field points are generated in ways closely related to some kinds of three dimension lattice; while in the latter case, the initial surface triangulation and the interior point distribution are more arbitrary.

For all the numerical examples, we compute several useful and indicative statistics of the resulting CVTs. They include: the energy per unit volume (E_p) discussed earlier, the *type-ratio*, and the quality of the dual Delaunay triangulation (the CVDT). The type-ratios T_r (ratio of the different types of Voronoi cells), in particular, the ratios of polyhedra with 12, 13, 14, 15, and 16 faces, are given as these Voronoi polyhedra typically account for almost all the Voronoi cells in a given CVT and these five types of cells also occupy most of the domain during the Lloyd iteration. The details of the type-ratio reveal much of the geometric structure of the CVT, for example, the type-ratio of a BCC-based CVTs is 0 : 0 : 1 : 0 : 0, which means that all the Voronoi cells are 14-faced polyhedra, (and careful examinations indicate that they are the truncated octahedra). The numerical values given in the paper for the type ratios are not normalized, so that they only provide a relative percentage, for instance, 0.1 : 0.1 : 1.0 : 0.1 : 0.1 would mean the same type ratio as 0.2 : 0.2 : 2.0 : 0.2 : 0.2. The element quality data on the centroidal Voronoi Delaunay triangulation (CVDT) show that the optimal CVTs in three-dimensional space can lead to high quality tetrahedral meshes. Here, for each tetrahedral element e , we use the quality measure defined by $Q(e) = 2\sqrt{6}R_{in}/h_{max}$ with R_{in} being the radius of the inscribed-sphere of the tetrahedron, and h_{max} the longest edge length. We start our investigation with simple lattice based CVTs and then move onto more general CVTs. We note that the statistics are collected via the implementation of algorithms specifically designed for our numerical investigations.

3.1. Properties of Lattices Based CVTs

Lattices based CVTs were widely used in vector quantization, coding theory, bubble and foam geometry [10,21–24]. Various methods for the construction of different kinds of lattices and their quantizations or CVTs have been reported in [21,23,25,26]. In [10], it was shown that the optimal lattice quantizer in three dimensions is the body-centered cubic (BCC) lattice based quantizer, i.e., the optimal lattice-based CVT cell is given by the truncated octahedron. Recently, a variant of the A15 lattice (so-called Weaire-Phelan partition) [23,25,27] was proposed in connection with the Kelvin conjecture (on the partition of R^3 with the least surface area). It has been shown in [10,23,25] that this A15 variant is inferior to the BCC in terms of both the value of E_p and the normalized moment of inertia (NMI).

To provide further numerical substantiation to the Gersho's conjecture, we design the following experiments: first, we compute the optimal CVTs from a set of initial conditions for a cubic domain via the Lloyd iteration. The cubic domain is scaled to be $[0, 10]^3$ without loss of generality. We first construct a series of lattice-based CVTs including cells represented by the FCC (the face centered cubic lattice), BCC, A15, and Z configurations. The A15 configuration here refers to the original partition, not the Weaire-Phelan partition. As most of the lattice-based CVTs are

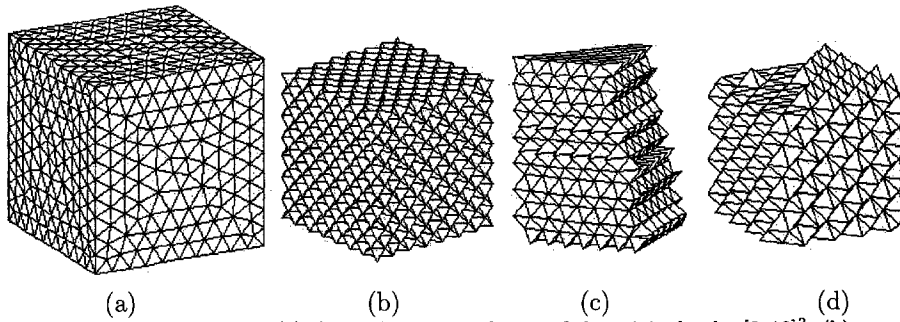


Figure 2. FCC lattice: (a) the surface triangulation of the original cube $[0, 10]^3$; (b) the FCC based surface triangulation for elements inside a smaller cube $[2, 8]^3$; (c) a cutting view of the interior Delaunay triangulation of the FCC lattice points; (d) a cutting view of the FCC based CVDT.

not exactly cube-filling, to minimize the boundary effect, we only collect the needed statistics from a smaller interior region away from the boundary. We also carry out similar computations for domains other than a cube such as cylinders and other composed domains.

With the cubic domain as a primary example, our computational procedure involves the following main steps:

- (1) the surface triangulation of the domain is first constructed with uniform sizing (as shown in Figure 2a for the cubic domain $[0, 10]^3$);
- (2) then, for a lattice based configuration, the inner field points are generated using the corresponding lattice (with the same sizing as the surface triangulation);
- (3) with the inner field points obtained above, an initial constrained three-dimensional Delaunay triangulation is generated via the method of constrained Delaunay insertion and associated boundary recovery procedure [3,28,29];
- (4) the elements contained in a smaller interior domain (for example, the smaller cube $[2, 8]^3$ inside the original cubic domain $[0, 10]^3$) are gathered to form a Delaunay triangulation whose dual configuration gives a Voronoi tessellation corresponding to the pure lattice points, without using any boundary points of the original larger domain (take the FCC as an example, Figure 2b shows a surface triangulation of the FCC based Delaunay mesh, while one of its cutting view is shown in Figure 2c);
- (5) finally, starting from this Delaunay mesh, the Lloyd iteration is performed until convergence to obtain the final CVT and its dual CVDT (Figure 2d shows a cutting view of an example given by the FCC-based CVDT).

We note that in our implementation of the Lloyd iteration, no movement of the boundary generators is allowed in order to preserve the boundary integrity.

The use of the lattice based initial field distribution is to study the stability of corresponding lattices, i.e., whether a lattice-based Voronoi tessellation leads asymptotically to a local or global minimum of the energy (and thus E_p), as well as their sensitivity to the boundary surface triangulation.

FCC. The face-centered-cubic (FCC) lattice is formed by the vertices of the regular cubic cells and their face centers with the corresponding Voronoi cell being a rhombic dodecahedron and the type-ratio $1 : 0 : 0 : 0 : 0$. The Voronoi tessellation of a FCC lattice is a CVT with $E_p = 0.07874$ and its dual Delaunay triangulation has two kinds of basic elements with element qualities at $Q = 0.656$ and $Q = 1.00$ respectively. The dihedral angles corresponding to the two basic elements are $[4(54.735), 1(90), 1(109.47)]$ and $[6(70.528)]$. The average mesh quality number is 0.7823. We note that in [30], it has been argued that the FCC was a preferred choice, comparing to the BCC, for an optimal finite-element mesh generation in terms of better approximation error bounds.

To study the stability of the FCC lattice based CVT, we first either make some random perturbations to the interior lattice points that lead to an initial FCC lattice Voronoi tessellation, or

replace these points with some other point distributions, then apply the Lloyd iteration to construct constrained CVTs. Similar experiments have been reported in [1] in the two-dimensional cases where it was demonstrated that the regular square lattice is less stable and it often transforms to the hexagonal lattice under initial perturbations and the Lloyd iteration.

For our experiments, we denote the case where the initial perturbations move the vertices by less than 10% of the local sizing as *PS* and the case where the perturbations move the vertices to as much as 50% of the local sizing as *PL*. The case *PC* denotes the case where the interior points are replaced by small random perturbations to points on a Cartesian grid with comparable number of vertices through an appropriate scaling.

Table 1. Statistics of FCC based CVTs and CVDTs with different initial distributions.

Case	Ini E_p	Ini T_r	Ini AQ	Final E_p	Final T_r	Final AQ
PS	0.07911	8.6:1.2:1.3:1.8:1.1	0.765	0.07874	18.6:0.2:0.3:0.2:0.1	0.779
PL	0.08029	2.6:2.2:3.5:1.8:2.1	0.747	0.07880	14.1:1.1:0.9:1.0:0.5	0.778
PC	0.08892	1.0:2.1:3.2:3.0:2.0	0.546	0.07879	15.2:1.3:1.1:0.3:0.5	0.779

In Table 1, the statistics of energy per unit volume (E_p), type-ratio (T_r), and the average element quality (AQ) show that the *PS* configuration leads to an iteration that eventually converges to the original FCC based CVT, thus, the FCC based Voronoi tessellation is locally stable. In comparison, when the perturbations are enlarged, the initial Voronoi tessellations become more nonlattice like and they are no longer close to the FCC structure, yet, the final CVTs after the Lloyd iteration are still very close to the FCC lattice. The third experiment shown in the Table 1 corresponds to an initial configuration quite different from the FCC structure, but to our surprise, the converged CVT still closely resembles the FCC lattice structure. These results seem to indicate that the FCC lattice based CVT is a very stable local minimum. Of course, based on E_p , it is known that it is inferior to the BCC, and thus cannot be the globally optimal CVT. Moreover, in Section 3, the FCC based CVT is compared with that based on the BCC and the results show that the BCC is more stable than the FCC. We note that for all of data collected, the experiments are conducted with at least two different scales (having different numbers of generators) which all yield similar numerical statistics even though only the data of the larger scale are shown in the table.

BCC. The body centered cubic (BCC) lattice consists of vertices of the cubic cells along with the cell centers with corresponding Voronoi tessellation cell being the truncated-octahedron, a configuration predicted to be optimal by two conjectures, the Gersho's three-dimensional conjecture [10] and the Kelvin conjecture [23,27]. The dual Delaunay tetrahedral element is subdivision invariant and has a high quality measure $Q = 0.866$. The basic element has dihedral angles $[4(60), 2(90)]$. This BCC based Delaunay triangulation is widely used for quality meshing [31].

The Voronoi tessellation of BCC is itself a CVT with $E_p = 0.07854$, and it is subdivision invariant. It was shown in [10] that it is the optimal single-cell lattice quantizer (or CVT) in three dimensions. Our numerical experiments provide further substantiation to the Gersho conjecture that the globally optimal CVT in three dimensions among both lattice and nonlattice based ones is asymptotically given by the BCC based CVT.

Similar to the experiments of FCC, a Delaunay tetrahedral mesh of the BCC lattice is computed for a cubic domain. Figure 3 shows the surface mesh of the Delaunay triangulation of the BCC and its cutting view. Since the BCC based Voronoi tessellation is also a CVT, we design the numerical examples with the following initial interior generator distributions:

- (1) perturbations to the BCC lattice points;
- (2) Cartesian grid distributions; and
- (3) initial points forming an FCC lattice.

Again, these experiments are repeated at two different scales.

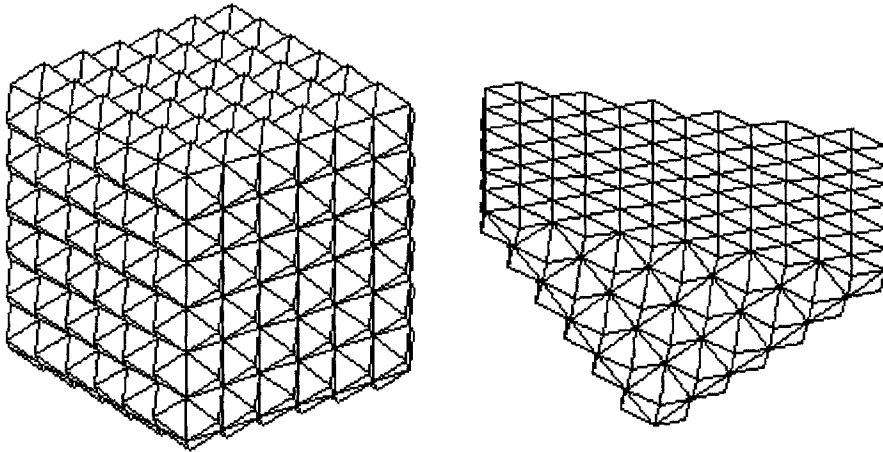


Figure 3. Surface triangulation of the BCC lattice and a cutting view of its Delaunay triangulation.

The first example intends to show the local stability of the BCC based CVT, thus, the interior points on the BCC lattice are given some small random perturbations, the data of the resulting tessellation are given in Table 2 (Case PS) which indicate that the initial VT is close to the BCC based CVT and the constructed CVTs in the later iterations converge to the original BCC based CVT.

By increasing the magnitude of the random perturbations to the initial interior point distribution, a configuration that is very different from the original CVT, is obtained, as indicated by the energy per unit volume E_p and the type ratio T_r in Table 2 (Case PL). Figures 4a and 4b display the cutting views of the dual Delaunay mesh for the initial VT and the final CVT. Note the Delaunay mesh shown in Figure 4a is very unstructured while the converged CVDT shown in Figure 4b is highly structured. Despite of the large perturbations, as in the FCC case, the converged CVTs still very closely resemble the BCC based one with $E_p = 0.07856$, the 14-hedra cell has the dominant percentage in the type ratios, and the tetrahedral mesh has a quality up to 0.857. The combination of these data again supports the BCC based CVT being the optimal CVT in three dimension.

Next, as in the experiments of the FCC, the initial interior points of the BCC lattice are replaced by points distributed on a Cartesian grid with a similar number of vertices through a suitable scaling. Again, the Lloyd iteration leads to the convergence to the BCC based CVT. The numerical data is given in Table 2 corresponding to the Case PC. Finally, the initial interior points are replaced by points forming a FCC lattice and the numbers of generators are adjusted as before. After the Lloyd iteration, the data (presented in Table 2, Case PF) of the resulting configurations give $E_p = 0.07857$, an average element quality 0.855 and a large type ratio of the 14-hedra, indicating the change from the FCC structure to the BCC structure during the

Table 2. Statistics of BCC based CVTs and CVDTs.

Case	Nodes	Ini E_p	Ini T_r	Ini AQ	Final E_p	Final T_r	Final AQ
PS	2630	0.07912	0.0:0.1:12.0:0.1:0.0	0.821	0.07854	0.0:0.0:1.0:0.0:0.0	0.866
PS	4789	0.07949	0.0:0.2:14.0:0.1:0.0	0.832	0.07854	0.0:0.0:1.0:0.0:0.0	0.865
PL	2566	0.08122	1.0:2.3:4.2:2.2:1.1	0.758	0.07858	0.1:0.3:12:0.3:0.2	0.854
PL	4928	0.08109	0.8:2.1:3.8:2.3:1.2	0.762	0.07856	0.05:0.2:14:0.1:0.1	0.857
PC	2533	0.08433	1.2:1.3:3.4:2.1:2.0	0.538	0.07860	0.1:0.3:10:0.4:0.2	0.848
PC	4859	0.08336	1.0:1.5:2.5:3.5:4.0	0.515	0.07861	0.1:0.2:12:0.2:0.3	0.850
PF	2735	0.08122	3.1:2.1:1.3:2.3:1.0	0.762	0.07857	0.1:0.5:22:0.3:0.15	0.855
PF	4864	0.08233	2.2:1.5:1.7:1.9:0.7	0.757	0.07857	0.05:0.3:19:0.2:0.13	0.854

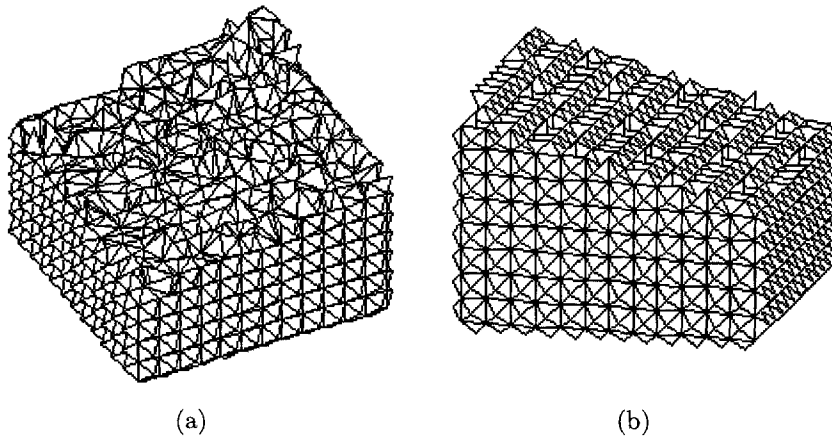


Figure 4. Cutting views of the initial DT (a) and CVDT (b) for FCC with a large initial perturbation.

Lloyd iteration. One may thus infer that the BCC is more stable than the FCC as the latter is transformed into the former (BCC) while the energy value gets lower.

A15 AND Z. The A15 lattice structure was discovered in the compound Na_8Si_{46} by Kasper *et al.* [26,32], and the Z lattice was observed in Zr_4Al_3 [33]. They are two fundamental TCP (tetrahedrally closed packed) structures [32,26] as all known TCP structures can be viewed as convex combinations of the three basic ones (A15, Z, C15). Here, only A15 and Z are considered. The basic cells of the A15 lattice based Voronoi tessellation contain one 12-hedron and three 14-hedra, while the basic cells of the Z lattice based VT are formed by three 12-hedra, two 14-hedra, and two 15-hedra. Thus, for the A15 and Z based Voronoi tessellations, the type-ratios are $1 : 0 : 3 : 0 : 0$ and $3 : 0 : 2 : 2 : 0$, respectively. The corresponding CVDT of A15 has three basic elements whose qualities are 0.9501, 0.907, 0.894, and the dihedral angles are $[3(67.79), 3(73.39)]$, $[2(72.97), 2(77.39), 63.43, 58.41]$, and $[4(78.46), 2(53.13)]$. The average element quality is up to 0.920 which is much larger than that of BCC based CVDT. And the minimal quality is 0.894. As for Z, its CVDT has five kinds of tetrahedra as well with the qualities 0.948, 0.931, 0.921, 0.919, 0.889 and dihedral angles $[4(77.07), 60, 53.13]$, $[2(71.01), 2(75.96), 63.43, 65.56]$, $[2(70.43), 2(71.63), 76.10, 63.82]$, $[3(73.89), 3(63.78)]$, and $[4(75.52), 2(60)]$. The average element quality is relatively smaller: $Q = 0.918$. Clearly, both the CVDTs of A15 and Z are acute tetrahedral meshes, which are also explored in [32].

Same as the FCC and BCC, both A15 and Z based Voronoi tessellations are themselves CVTs. For A15, $E_p = 0.07871$ which is smaller than that of FCC, and for Z, $E_p = 0.07910$ is slightly larger. Similar to the FCC experiments, the surface triangulations of A15 (or Z) based CVDTs and their perturbed or replaced interior points are taken as initial conditions for Lloyd iterations. The final convergence results in Table 3 show that both A15 and Z based CVTs are very stable local minima, like FCC and BCC. As for E_p , it is obvious that BCC is superior to Z, but A15

Table 3. Statistics of the A15 and Z based CVTs and CVDTs with different initial distributions.

Input	Dist.	Ini E_p	Ini T_r	Ini AQ	Final E_p	Final T_r	Final AQ
A15	PS	0.07873	1.0:0.1:3.0:0.0:0.0	0.914	0.07871	1.0:0.0:3.0:0.0:0.0	0.918
A15	PL	0.08309	1.0:2.2:2.9:3.0:2.3	0.689	0.07879	1.0:0.1:3.0:0.1:0.0	0.907
A15	PC	0.08593	1.0:1.8:2.9:2.1:2.0	0.656	0.07876	1.0:0.2:2.9:0.2:0.1	0.911
Z	PS	0.07931	3.0:0.1:2.0:2.0:0.1	0.908	0.07913	3.0:0.0:2.0:2.0:0.0	0.921
Z	PL	0.09026	1.0:1.2:1.3:1.1:1.2	0.586	0.07918	3.0:0.1:2.0:2.1:0.1	0.917
Z	PC	0.08692	1.0:2.1:4.2:3.8:2.0	0.532	0.07924	3.0:0.3:2.1:1.9:0.1	0.903

also stays competitive with the BCC. It not only has a low energy, but also has a high quality CVDT (with a quality measure up to 0.920). This warrants further comparisons.

We note that for the A15 based Weaire-Phelan partition, it was computed in [23,25,27] that $E_p \approx 0.078735$ which is a little smaller than that of the FCC, but is still larger than that of BCC. In [25], a different quantizer based on A15 was proposed, but it was also found inferior to the BCC.

COMPARISONS OF FCC, A15, Z, AND BCC. To make further comparisons of the BCC lattice with the FCC, A15, and Z, the original cube $[0,10]^3$, instead of the cutting-cube, is used to construct CVTs. Different initial field points are used to generate the four lattices respectively in the interior, but the boundary surface triangulations are kept the same. The Lloyd iterations are performed.

We report the experimental data in Table 4. As one can see from the table, the result of the FCC case is no longer a FCC based CVT. The data corresponding to the BCC are also shown there, and the final CVT is close to the BCC based CVT. Examining in details, it is found that the central part of BCC based CVT is hardly affected, while that of the FCC is very different from the initial one. This gives another indication of superiority of BCC over FCC. As for the A15, and Z, the final results contained in Table 5 indicate that Z is less stable than A15, and the final CVT is very different from the Z based CVT, while the results of A15 are still close to the A15 based CVT to some degree. Similar to the BCC, careful examination demonstrates that the central part of both A15 and Z based CVTs are not affected, which means that A15 and Z are also very stable, just as the BCC.

As A15 and BCC based CVTs have very close values of E_p , to further investigate their stabilities, numerical experiments are conducted in two directions. The surface triangulation of A15 based CVDT is first used during the Lloyd iteration. The initial interior point distribution is the BCC lattice. In a small scale, the final result of the Lloyd iteration is very close to a A15 lattice based CVT. The energy is 0.07874, the type ratio is 1.0 : 0.1 : 2.8 : 0.2 : 0.1, and the element quality is high (up to 0.913), as shown in Table 6 (Surface type A15). This might indicate that, in small scale, the A15 fares better than the BCC lattice, however, as the number of nodes increases, the story changes. In a larger scale with 4264 nodes, the final results show that the

Table 4. Statistics of a cube's CVTs with FCC and BCC initial distributions.

Case	Nodes	Ini E_p	Ini T_r	Ini AQ	Final E_p	Final T_r	Final AQ
FCC	1617	0.08155	6.4:1.3:1.1:2.0:0.5	0.776	0.07915	0.1:13:33:12:0.15	0.807
FCC	4459	0.08147	8.3:1.1:1.0:1.6:0.7	0.774	0.07913	0.2:14:36:12:0.23	0.812
BCC	1625	0.07886	0.1:1.0:1.1:1.4:0.0	0.860	0.07899	1.2:2.1:8.0:2.3:1.1	0.818
BCC	4330	0.07868	0.0:0.3:16:0.3:0.0	0.865	0.07871	0.4:2.1:15:1.2:0.3	0.823

Table 5. Statistics of a cube's CVTs with A15 and Z type initial distributions.

Input	Ini E_p	Ini T_r	Ini AQ	Final E_p	Final T_r	Final AQ
Z	0.07925	2.9:0.2:2.1:2.0:0.1	0.895	0.07934	1.0:0.4:1.4:1.1:0.2	0.871
A15	0.07876	1.0:0.1:2.9:0.1:0.0	0.889	0.07898	1.0:0.2:2.6:0.1:0.05	0.853

Table 6. Statistics of CVTs with A15 and BCC based surface triangulation with alternate BCC and A15 type initial distributions.

Surf	Input	Nodes	Ini E_p	Ini T_r	Ini AQ	Final E_p	Final T_r	Final AQ
A15	BCC	1531	0.07884	0.3:1.0:7.2:1.2:0.5	0.847	0.07874	1.0:0.1:2.8:0.2:0.1	0.913
A15	BCC	4264	0.07879	0.1:1.0:9.0:0.4:0.3	0.852	0.07870	1.5:1.5:8.6:1.5:0.4	0.840
BCC	A15	1558	0.08122	1.0:0.2:2.6:0.2:0.1	0.863	0.07856	0.0:0.3:20:0.2:0.0	0.860
BCC	A15	4789	0.08081	1.0:0.3:2.8:0.1:0.1	0.898	0.07858	0.1:0.2:18:0.3:0.1	0.859

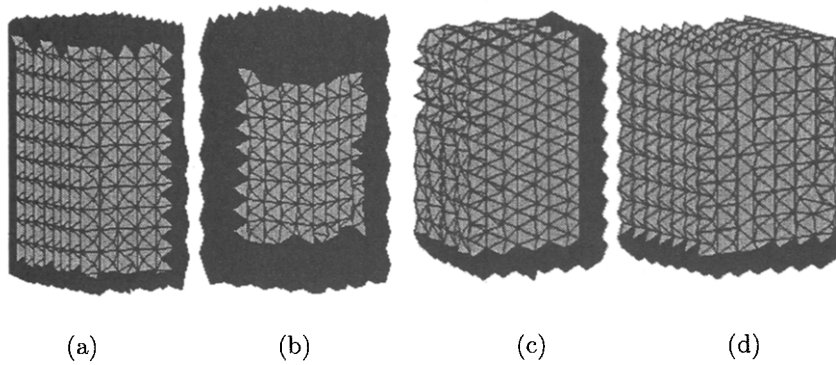


Figure 5. Cutting views of the initial DT (a), CVDT (b) for A15, and the initial DT (c) and CVDT (d) for BCC.

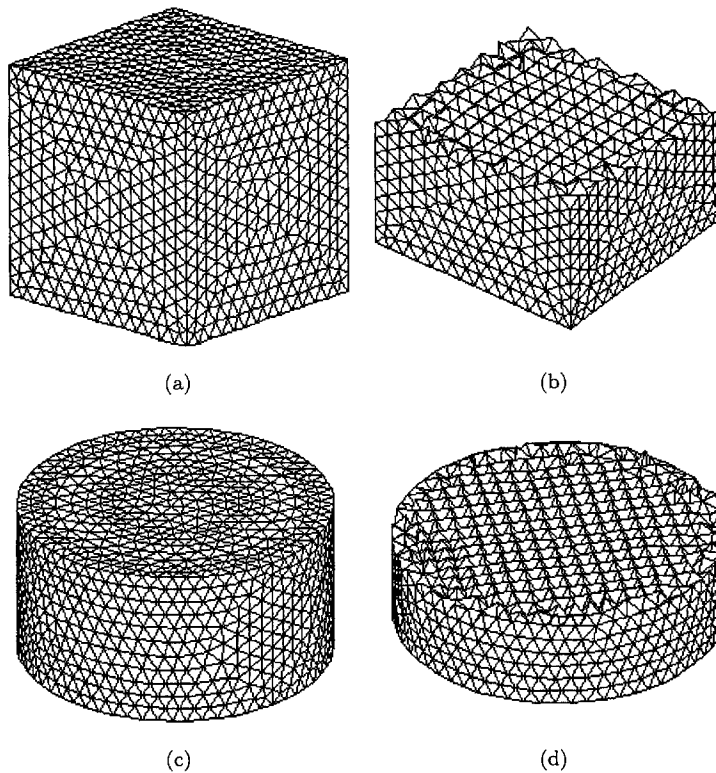


Figure 6. The CVDTs of a cube and a cylinder with initial BCC distributions: (a),(b) surface triangulation; (c),(d) cutting views of the final CVDTs.

interior BCC lattice *defends* vigorously against the attacking A15. The final type ratio retains a 14-hedra dominance and the central part of the CVDT is still BCC based tetrahedral mesh. Figures 5a and 5b show the cutting views of the initial DT and final CVDT with a BCC based configuration clearly shown and it is clearly shown in Figure 5b, the green central part is still of a BCC lattice based mesh structure.

On the contrary, when the A15 lattice is used as the initial distribution along with a BCC based surface triangulations, in both small and large scales, the Lloyd iterations converge to BCC based CVTs. Table 6 contains the statistics corresponding to Surface type BCC and Figures 6a and 6b give the cutting views of the meshes (note the changes from an A15 based mesh to a BCC based one). This means that, asymptotically, the BCC is more robust than the A15 under perturbations of different kinds, thus adding evidence to the conclusion that BCC is more stable than A15.

So far, we have compared four kinds of lattice based CVTs. The stability properties and other related data adds to the superiority of the BCC based CVT over the others which was first established through the analysis of the energy per unit volume [10] among all lattice based CVTs with a single congruent cell. Moreover, they also substantiate the conclusion that the BCC based CVT is optimal among all lattices, not only among the CVTs corresponding to lattices with only one type of congruent Voronoi cells [10]. The investigation on nonlattices CVTs will be made next.

3.2. Properties of Nonlattice CVTs

The nonlattice examples to be presented next include different domains and different initial conditions: surface triangulations and initial point distributions including AFT-type, randomized Cartesian grid points distributions. The different domains are, a cube, a cylinder, a Par6 domain which is formed by a convex set of BCC based Delaunay tetrahedra, and a concave domain made of two Par6 domains. The properties of the CVTs of these domains along with different initial interior point distributions are to be examined here.

A CUBE AND A CYLINDER. To generate nonlattice CVTs, the cube $[0, 10]^3$ is first meshed by the constrained Delaunay method with an almost equilateral surface triangulation and interior field points generated by the advancing front technique. Then the Lloyd iterations are performed to obtain the converged CVT. Numerical computations are conducted at three different scales. Table 7 shows the numerical results of the initial VTs and the generated CVTs (corresponding to the cube being the input). Similar experiments are done for a cylinder with results shown in the same table (corresponding to the cylinder being the input). From the table, we can see that all the CVTs have energy per unit volume values larger than 0.07910, thus, larger than that of the BCC based CVT. Also, the type ratios favor the portion of the 14-hedra, whose number is almost equal to the sum of all other kinds. But the element qualities are significantly better than those of the initial triangulations, with increases from about 0.660 and 0.640 to 0.812 and 0.807 respectively (still smaller than 0.866 of the BCC based CVDT elements). In other words, these CVTs are inferior to the BCC based ones, though they show some tendency to converge to the optimal one.

As a further demonstration, the initial points of the above Voronoi tessellations are replaced with points forming a BCC lattice of the same number of generators. The numerical data of the

Table 7. Statistics of CVTs for a cube and a cylinder with an AFT initial distribution.

Input	Nodes	Ini E_p	Ini T.Ratio	Ini AQ	Final E_p	Final T.Ratio	Final AQ
Cube	2216	0.08399	1.0:0.8:2.5:3.0:2.8	0.666	0.07924	1.0:5.3:12:4.3:1.0	0.812
Cube	4227	0.08382	1.0:1.3:2.8:3.1:2.9	0.661	0.07920	1.0:5.0:11:4.2:0.6	0.812
Cube	9420	0.08343	1.0:1.5:1.8:2.9:2.9	0.657	0.07914	1.0:4.3:13:3.6:0.7	0.813
Cylinder	2742	0.08544	1.0:1.8:2.7:3.1:2.0	0.646	0.07940	1.0:4.0:9.2:3.1:1.1	0.807
Cylinder	3923	0.08477	1.0:1.7:2.4:2.0:1.3	0.639	0.07942	1.0:3.6:8.1:4.0:1.2	0.806
Cylinder	8173	0.08552	1.0:1.8:2.5:2.6:1.7	0.645	0.07935	1.0:4.0:9.7:3.4:1.4	0.808

Table 8. Statistics of CVTs for a cube and a cylinder with a BCC initial distribution.

Input	Nodes	Ini E_p	Ini T.Ratio	Ini AQ	Final E_p	Final T.Ratio	Final AQ
Cube	1625	0.07886	0.1:1.0:11:1.4:0.0	0.860	0.07899	1.2:2.1:8.0:2.3:1.1	0.818
Cube	4330	0.07868	0.0:0.3:16:0.3:0.0	0.865	0.07871	0.4:2.1:15:1.2:0.3	0.823
Cube	8733	0.07864	0.0:0.2:21:0.1:0.1	0.866	0.07866	0.3:1.2:17:2.1:0.1	0.834
Cylinder	1733	0.07894	0.4:2.3:9.4:2.5:0.4	0.843	0.07921	1.0:3.3:9.4:3.4:0.8	0.808
Cylinder	4554	0.07870	0.2:1.1:11:1.3:0.3	0.857	0.07882	0.3:2.0:13:1.8:0.5	0.818
Cylinder	7988	0.07864	0.0:0.5:19:0.3:0.0	0.863	0.07869	0.3:1.8:16:1.1:0.2	0.830

converged CVTs are shown in Table 8. Figure 6 shows the boundary surface triangulations and the cutting views of the final CVDTs. Both the data and the meshing structures in Figures 6b and 6d clearly demonstrate that in the Lloyd iteration, much of the initial BCC lattice remain unchanged, and the final CVTs are almost the same as the initial VTs.

PAR6 DOMAIN AND A COMPOSITIONAL PAR6 DOMAIN. To investigate the influence of the boundary surface triangulation on the Lloyd iteration, i.e., to the quality of the converged CVTs, more examples with three different scales of nodes are carried out in the following manner:

- (1) a parallelepiped domain is cut from the BCC lattice based Delaunay triangulation, as shown in Figure 7a, and it is called a Par6 domain;
- (2) substitute the field points by Cartesian grid points along with random perturbations, whose Delaunay triangulation is shown in Figure 7b (with very low mesh quality, as shown in Table 9); and
- (3) a CVT is constructed with the Lloyd iteration.

From Table 9 (for Par6 being the input) and the CVDT mesh in Figure 7, it can be concluded that the computed CVT is virtually similar to the BCC based CVT. It has a low value of $E_p = 0.07860$, a 14-hedra dominant ratio $0.2 : 1.0 : 23 : 1.0 : 0.2$, and a high quality CVDT. The above example shows a transition from an initial nonlattice Voronoi tessellation (in Figure 7b) to the BCC lattice based CVT (in Figure 7c) during the Lloyd iteration, provided a BCC conforming surface triangulation is used.

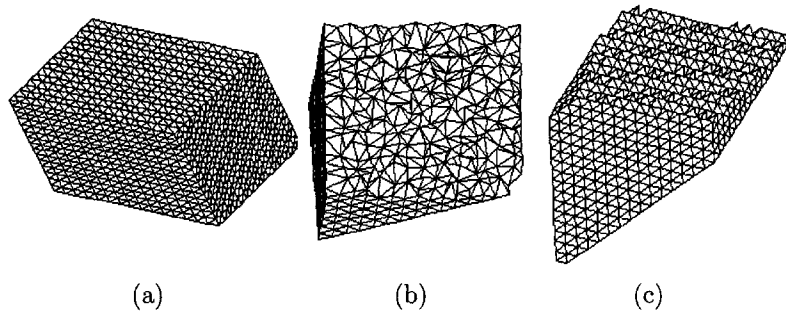


Figure 7. CVDT meshing of a Par6 Domain: (a) surface triangulation; (b) the cutting view of the initial Delaunay triangulation; and (c) the cutting view of the final CVDT.

Table 9. Statistics of Par6 and CD with a Cartesian initial distribution with small random perturbation.

Input	Nodes	Ini E_p	Ini T.Ratio	Ini AQ	Final E_p	Final T.Ratio	Final AQ
Par6	2331	0.08522	1.0:2.2:3.1:4.5:4.0	0.520	0.07865	0.2:1.0:24:1.1:0.3	0.846
Par6	4096	0.08644	1.0:1.8:2.7:3.7:4.2	0.524	0.07866	0.2:1.0:23:1.0:0.4	0.844
Par6	8000	0.08671	1.0:2.1:2.8:4.2:4.9	0.525	0.07867	0.3:1.0:23:1.2:0.2	0.844
CD	2655	0.08878	1.0:1.9:2.9:2.7:3.9	0.525	0.07868	0.1:1.0:16:1.0:0.1	0.841
CD	4132	0.08876	1.0:1.8:2.7:3.0:3.6	0.523	0.07867	0.3:1.0:15:1.1:0.1	0.839
CD	8432	0.08890	1.0:1.7:2.9:2.9:3.3	0.526	0.07870	0.2:1.0:15:1.1:0.3	0.840

Adding up two axis-symmetric Par6 domains and their corresponding meshes, a concave domain (CD) is obtained together with a mesh. Its surface triangulation is shown in Figure 8a. Obviously it is BCC compatible. As in the Par6 case, the initial interior points are replaced with randomly perturbed Cartesian grid points and Lloyd iterations are performed. Table 9 (with CD being the input) contains the numerical data and Figure 8 shows the initial DTs and CVDTs. Similarly, one can conclude as in the previous case that the final result is like the BCC based CVT shown in Figure 8c, thus providing more evidence to the validity of the Gershov's conjecture in three dimensions.

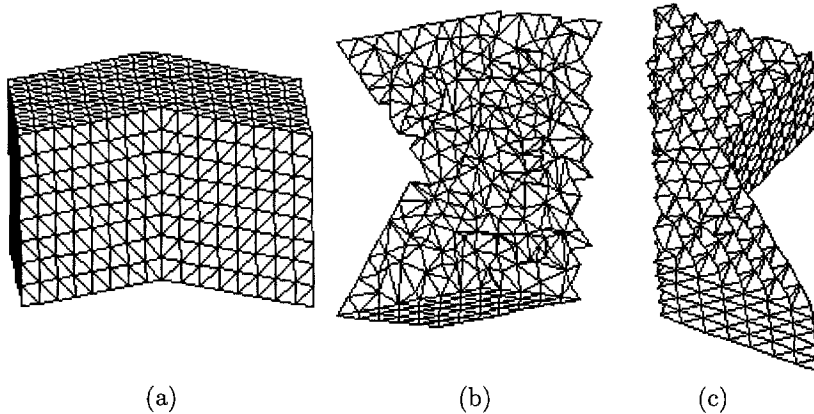


Figure 8. CVDT meshing of a composed Par6 domain: (a) surface triangulation; (b) the cutting view of the initial Delaunay triangulation; and (c) the cutting view of the final CVDT.

4. SENSITIVITY OF THE LLOYD ITERATION

From the numerical examples in Section 3 and the analyses of the numerical results, it can be drawn that for a given three-dimensional domain, the Lloyd iteration method can be applied to obtain the optimal CVT, provided that the initial conditions are *good* in the sense that the boundary surface triangulations and the initial field point distribution are in good conformity with the BCC lattice. If the initial conditions for the Lloyd iteration are *not good*, the final results may be stuck in some local minima, and thus, be different from the optimal BCC based CVT. We refer this as the *sensitivity* of the Lloyd iteration. In this section, more experiments are performed to examine such a notion.

4.1. Gradual Modification of Boundary Surface Triangulations

The composed Par6 domain derived from the BCC lattice in Section 3 is used to construct a sequence of CVTs with different initial conditions for the Lloyd iterations. The initial field point distribution is fixed to be the Cartesian grid type with possibly small random perturbations. The boundary surface triangulations are changed gradually, resulting in different final results, i.e., different CVTs. Initially, the surface triangulation of the compositional par6 domain, which is in conformity with the BCC lattice, is re-meshed by edges contractions/splitting and nodes smoothing [34,35]. The replaced mesh is a Delaunay-type surface triangulation with a similar sizing. Figure 9a shows the re-meshed surface mesh. Then, the re-meshed areas of the boundary surface are gradually decreased. The second example has two facets and their neighboring elements re-meshed, the third example has only one facet and its neighboring elements re-meshed, and the final one keeps the initial surface triangulation unchanged. Figure 9 shows the sequence of changes to the boundary surface triangulations. With similar initial Cartesian type point distributions, the four different CVTs corresponding to these four boundary surface triangulations are constructed via the Lloyd iterations. The cutting views of the four final CVDTs are shown in Figures 10a–10d. For all the examples, Lloyd iterations with two different scales of nodes are performed. The numerical data of the larger scale with the number of nodes being 7862 are presented in Table 10, where *Null*, *Half*, *OverH*, and *All* means that no facet, one facet with some neighboring elements, two facets with some neighboring elements, and all the boundary surfaces are in conformity with BCC respectively. The data of the initial VTs and their Delaunay meshes show that all the initial Voronoi tessellations are far from the optimal BCC based CVTs. With the changes of the boundary surface triangulations from BCC noncompatible ones to BCC compatible ones, the numerical data of the final CVTs and CVDTs are gradually converging to those of the BCC based CVT. Note the gradual changing of the mesh structures of

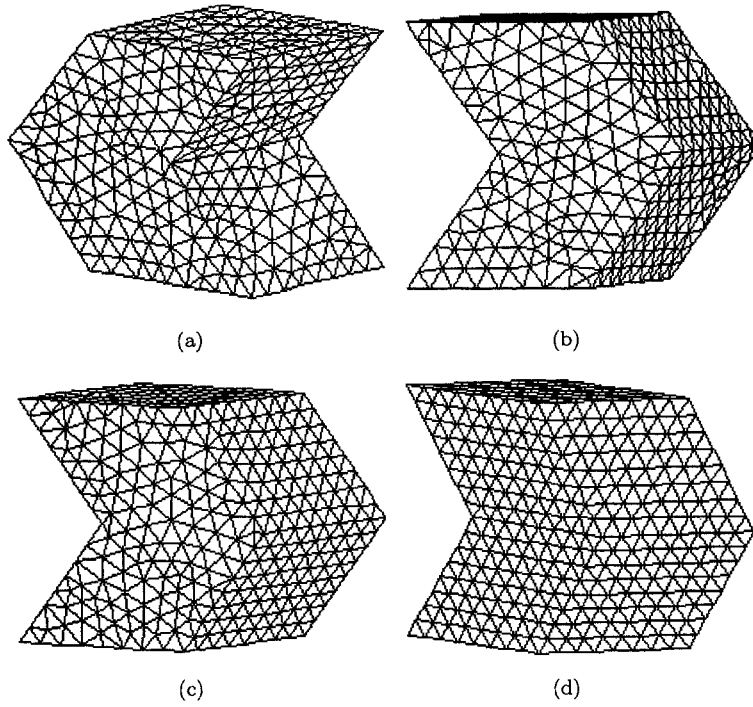


Figure 9. Different surface triangulations for the Lloyd iterations: (a) all facets remeshed; (b) two facets remeshed; one hidden; (c) one facet remeshed; and (d) all initial surface triangulation kept unchanged.

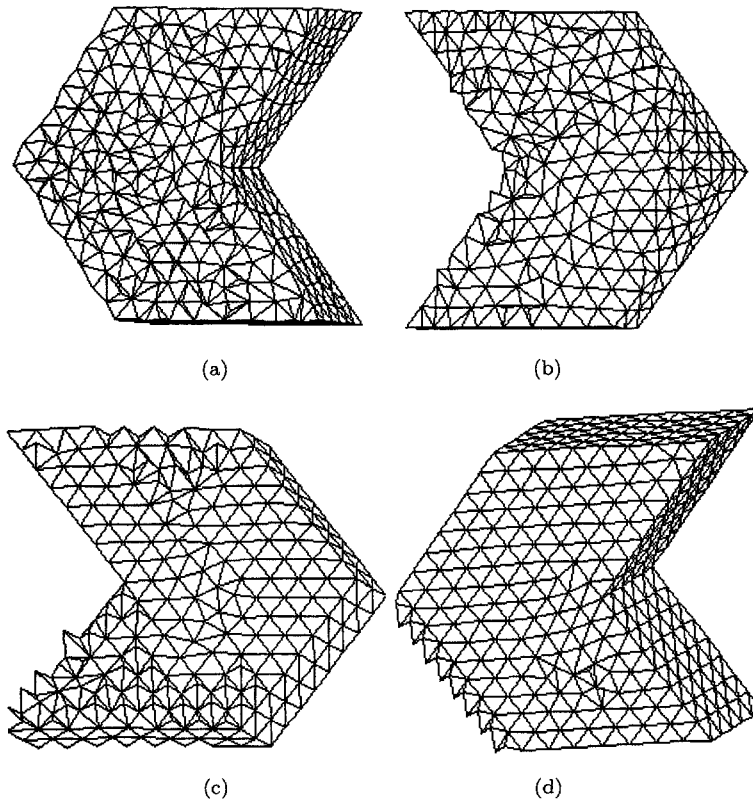


Figure 10. Cutting views of CVDTs corresponding to the different surface triangulations in Figure 9.

Table 10. Statistics of a composed domain with gradual modifications of surface triangulations and perturbed Cartesian initial distributions.

D.Surf	Ini E_p	Ini T.Ratio	Ini AQ	Final E_p	Final T.Ratio	Final AQ
Null	0.1002	1.0:1.6:1.7:2.0:1.8	0.567	0.07941	0.3:1.0:2.7:1.1:0.2	0.788
Half	0.0997	1.0:1.5:2.1:2.1:2.1	0.564	0.07905	0.2:1.0:5.7:0.8:0.1	0.810
OverH	0.1012	1.0:1.6:2.1:2.4:2.1	0.578	0.07876	0.1:1.0:11:0.9:0.1	0.827
All	0.0982	1.0:1.6:2.1:2.3:2.3	0.564	0.07869	0.2:1.0:15:1.0:0.1	0.841

the CVDTs from very unstructured one shown in Figure 10a to structured BCC lattice based one shown in Figure 10d. The E_p decreases from 0.07941 to 0.07869, the type-ratio changes from 0.3 : 1.0 : 2.7 : 1.1 : 0.2 to 0.2 : 1.0 : 15 : 1.0 : 0.1, and the average quality increases from 0.788 to 0.841. The sensitivity of the Lloyd iteration to the boundary surface mesh is thus clearly observed. This works as a further proof to the asymptotic trend from a nonlattice CVT to a BCC lattice based CVT.

4.2. A Cube with Not-So-Good Initial Conditions

As another investigation on the sensitivity of the Lloyd iteration to the initial conditions, the cube $[0, 10]^3$ is taken again to construct CVTs of different scales. The surface triangulations are uniform sizing and almost equilateral as in Section 3. Also, the initial field points are generated with the AFT techniques as before and are randomly perturbed. However, to probe the asymptotic property, the numbers of nodes are chosen to be 23824, 46277, and 79000, which are much larger than before. Obviously, the initial conditions do not resemble the BCC lattice and the final results of the Lloyd iterations may be different from the BCC lattice structure, as shown before. However, since the scales are larger, asymptotically, we are expecting a BCC-like structure appearing in the central part of the cube where the influence of the boundary surface triangulation is less significant. For this, the numerical data of the central part($[3, 7]^3$) of the CVT and CVDTs are chosen for analysis and are presented in Table 11.

Table 11. Statistics of central part of CVTs and CVDTs in a cube.

Nodes	C.I E_p	C.I T.Ratio	C.I AQ	C.F E_p	C.F T.Ratio	C.F AQ
23824	0.08379	1.0:1.4:1.8:1.9:1.1	0.679	0.07914	0.3:1.0:2.5:1.3:0.1	0.817
46277	0.08433	1.0:2.0:3.0:2.4:1.8	0.659	0.07905	0.1:1.0:3.0:1.1:0.2	0.818
79000	0.08416	1.0:1.3:1.5:2.0:1.5	0.666	0.07901	0.2:1.0:3.4:1.2:0.4	0.820

The notation “C.I E_p ” in Table 11 represents the E_p of the central part of the initial Delaunay triangulation, while “C.F E_p ” is the E_p of the central part of the final CVDT. Others can be interpreted accordingly. From the statistics of the energy per unit volume of the final CVTs, it can be seen that there is a tendency to approach the optimal BCC structure. The E_p decreases from 0.07914 to 0.07901 accompanied by the increase of the average quality. The type ratios clearly say that it is still far from the optimal BCC lattice based CVT. As the current Lloyd iteration converges very slowly, it is formidable to construct larger scales, such as 200000 or more. Towards this end, several speeding up techniques, such as localizing and parallelizing the Lloyd iteration, are under development [17,36].

As a conclusion, from the applications point of view, it is not pragmatic to seek for a CVT with a *bad* initial conditions. For a given domain and a sizing specified, the most feasible way to construct its optimal CVT is to mesh the boundary surface with triangulations as regular as possible, generate the inner field points with the BCC lattice, and perform the Lloyd iterations. The resulting CVT is very close to the optimal BCC lattice based CVT, and will have nice qualities for wide applications, which will be probed in the next section. Also, in order to make the boundary influence effects further clear, it could be promising to examine periodic boundary

conditions which means to solve the problem in a unit cube of a tessellation and this will be investigated in the future.

5. APPLICATION OF OPTIMAL 3D CVTS

The optimal three-dimensional CVT, i.e., the BCC lattice based CVT has a lot of optimal qualities. The lowest energy per unit volume (0.078543) makes it the best quantizer in vector quantization and coding theory. There are many other applications of the optimal CVTs in image analysis, computer graphics, resource allocation, astronomy and biology, see [1]. From the above experiments, we can also see that the optimal CVT is highly structured and the data structure can be simplified compared with nonlattice based CVTs.

Corresponding to the optimal 3D CVT, the dual Delaunay mesh, i.e., the CVDT also enjoys many nice properties [3]. Indeed, the BCC lattice has been applied to quality 3D meshing in the literature, see for instance [32] which gives a structured tetrahedral mesh with high quality 0.866. The BCC based mesh also has the lowest elements edges length ratio [32] among all lattice based mesh, making it the most regular uniform 3D mesh. The subdivision invariance of such a mesh also makes it useful for multigrid methods. As each tetrahedron has two 90° dihedral angle, it is only a nonobtuse tetrahedral mesh [32], while A15 and Z based CVDTs enjoys the acuteness qualities. However, as A15 and Z are less stable than BCC and their CVDTs are not as structured as that of BCC, it is preferred to apply the BCC for quality meshing without the acuteness requirement.

In application, the geometry is usually complicated and constructing a completely BCC-like mesh is not feasible. Thus, the CVDT often gives a good approximation. Careful examination of the CVDTs constructed in our earlier experiments shows that the CVDT meshes have many common characteristics. First, the meshes all have edge length ratios smaller than 1.8 and the largest edge length ratio for any element is less than 1.56. Moreover, measuring in the *radius-edge ratio* (the ratio of the circum-radius to the shortest edge length of the tetrahedron), the mesh is obviously an *almost good mesh* [14,37]. Therefore, only *sliver elements* are of bad quality (takes as those with a quality less than 0.3). In addition, many of these sliver elements are close to the boundary, and their number may be reduced by good initial distributions of vertices near the boundary. Among the sliver tetrahedra, they all have four shorter edges and two longer edges. The latter ones are opposite to each other and almost coplanar, with each connecting less than five tetrahedra and only one sliver element emanating from it. Thus, there are no clustered sliver elements so that each sliver element can be killed by a simple edge/face swapping [3], which explains the high quality mesh examples given in [3].

In summary, as an application of optimal CVT, a procedure for high quality uniform isotropic three-dimensional tetrahedral meshing of a given complicated geometry can be implemented through the following steps:

- (1) generate an almost equilateral surface triangulation of the geometry via existing meshing technique and optimized with approximate surface CVT techniques [17];
- (2) use one or two layers of points via AFT technique first along the boundary then match with BCC lattice type points in the interior;
- (3) perform Lloyd iterations to construct the CVDT; and
- (4) apply simple edges/faces swaps for sliver elements deletion.

Of course, when the dihedral acuteness is a necessity in application, the use of A15 type points may be favored in place of the BCC lattices in the above procedure. We leave more detailed discussions in our future work [36].

6. CONCLUSIONS AND FUTURE WORKS

In this paper, we made numerical investigations on the optimal centroidal Voronoi tessellations and the Gershgorin's conjecture in the three-dimensional spaces. Based on the simulation results,

some conclusions are in order. We first note that the optimal CVT studied here is a special type of CVT corresponding to a constant density. Optimal CVTs for more general densities can also be studied [1], although asymptotically speaking, if the density function is smoothly varying in space and the number of generators is very large, the density function may be viewed as a constant function on a local scale, and the centroidal Voronoi cells locally will be close to that for the constant density. Thus, our study here also bears significance to the optimal CVT for more general density functions. Next, through the numerical experiments here, the three-dimensional Gershgorin conjecture is further substantiated and the BCC based CVT is shown to be the most possible congruent cell, numerically. The experiments also demonstrate that the Lloyd iteration can be applied to get the optimal solution under good initial conditions but they may also get stuck at local minima starting from some other initial conditions. Moreover, in this paper, the good qualities of the CVT and CVDT are also demonstrated which are useful for high quality 3D meshing.

In the future, further evidence may be gathered for the validity of the Gershgorin conjecture through the improvement of the Lloyd type iterations for the construction of CVTs on even larger scales and through other theoretical and numerical analysis. Such studies will be useful also to the successful applications of CVTs in many scientific and engineering areas [1].

REFERENCES

1. Q. Du, V. Faber and M. Gunzburger, Centroidal Voronoi tessellations: Applications and algorithms, *SIAM Review* **41**, 637–676, (1999).
2. Q. Du and M. Gunzburger, Grid generation and optimization based on centroidal Voronoi tessellations, *Applied and Computational Mathematics* **133**, 591–607, (2002).
3. Q. Du and D. Wang, Tetrahedral mesh generation and optimization based on centroidal Voronoi tessellations, *Int. J. Num. Method. Engrg.* **56**, 1355–1373, (2003).
4. Q. Du, M. Gunzburger and L. Ju, Meshfree, probabilistic determination of point sets and support regions for meshless computing, *Comput. Methods Appl. Mech. Engrg.* **191**, 1349–1366, (2002).
5. Q. Du, M. Gunzburger, L. Ju and X. Wang, Centroidal Voronoi tessellation algorithms for image compression and segmentation, (preprint).
6. A. Hausner, Simulating decorative mosaics, In *Proc. 28th Annual Conference on Computer Graphics and Interactive Techniques*, pp. 573–580, (2001).
7. T. Kanungo, D. Mount, N. Netanyahu, C. Piatko, R. Silverman and A. Wu, An efficient k-means clustering algorithm: Analysis and implementation, *IEEE Trans. Pattern Anal. Machl Intel.* **24**, 881–892, (2002).
8. A. Gershgorin, Asymptotically optimal block quantization, *IEEE Trans. Inform. Theory* **25**, 373–380, (1979).
9. D. Newman, The Hexagon theorem, *IEEE Trans. Infor. Theory* **28**, 137–139, (1982).
10. E.S. Barnes and N.J.A. Sloane, The optimal lattice quantizer in three dimensions, *SIAM J. Algebraic Discrete Methods* **4**, 30–41, (1983).
11. R.M. Gray and D.L. Neuhoff, Quantization, *IEEE Trans. Inform. Theory* **44**, 2325–2383, (1998).
12. S. Lloyd, Least square quantization in PCM, *IEEE Trans. Infor. theory* **28**, 129–137, (1982).
13. Q. Du, M. Emelianenko and L. Ju, Convergence properties of the Lloyd algorithm for computing the Centroidal Voronoi Tessellations, (preprint).
14. J.R. Shewchuk, Tetrahedral mesh generation by Delaunay refinement, In *Proceedings of the 14th Annual ACM Symposium on Computational Geometry*, pp. 86–95, (1998).
15. G.L. Miller, D. Talmor, S.H.Teng and N.Walkington, A Delaunay based numerical method for three dimensions: Generation, formulation and partition, In *Proc. 27th A. ACM Sympos. Theory Computing*, pp. 683–692, (1995).
16. Q. Du, M. Gunzburger and L. Ju, Constrained centroidal Voronoi tessellations on general surfaces, *SIAM J. Sci. Comp* **24** (5), 1499–1506.
17. Q. Du and D. Wang, Approximate Constrained centroidal Voronoi tessellation on surfaces and the application to surface mesh optimization, (preprint).
18. Q. Du, M. Gunzburger and L. Ju, Probabilistic methods for centroidal Voronoi tessellations and their parallel implementations, *Journal of Parallel Computing* **28**, 1477–1500, (2002).
19. J. MacQueen, Some methods for classification and analysis of multivariate observations, In *Proc. Fifth Berkeley Symposium on Mathematical Statistics and Probability, I*, (Edited by L. LeCam and J. Neyman), pp. 281–297, (1967).
20. A. Jain and R. Dubes, *Algorithms for Clustering Data*, Prentice Hall, Englewood Cliffs, NJ, (1988).
21. N.J.A. Sloane and V.A. Vaishampayan, A zador-like formula for quantizers based on periodic tilings, *IEEE Trans. Infor. Theory* **48**, 3138–3140, (2002).
22. J.H.Conway and N.J.A. Sloane, Voronoi regions of lattices, second moments of polytopes and quantization, *IEEE Trans. Inform. Theory* **28**, 211–226, (1982).

23. R. Kusner and J.M. Sullivan, Comparing the Weaire-Phelan equal-volume foam to Kelvin's foam, *Forma* **11**, 233–242, (1996).
24. J.M. Sullivan, The geometry of bubbles and foams, In *Foams and Emulsions (NATO ASI Volume E 354)*, pp. 379–402, Kluwer, (1999).
25. N. Kashyap and D. L. Neuhoff, On quantization with the Weaire-Phelan partition, *IEEE Trans. Inform. Thy.* **47**, 2538–2543, (2001).
26. J.M. Sullivan, New tetrahedrally close-packed structures, In *Foams, Emulsions and their Applications, Proceedings of Eurofoam*, pp. 111–119, Delft, (2000).
27. D. Weaire and R. Phelan, A counter-example to Kelvin's conjecture on minimal surfaces, *Phil. Mag. Lett.* **69** (2), 107–110, (1994).
28. Q. Du and D. Wang, Boundary recovery for three dimensional conforming Delaunay triangulation, *Computer Methods in Applied Mechanics and Engineering* **193**, 2547–2563, (2003).
29. Q. Du and D. Wang, Constrained boundary recovery for three dimensional Delaunay triangulations, *Int. J. Num. Method Engrg.* **61**, 1471–1500, (2004).
30. R. Radovitzky, M. Ortiz, Tetrahedral mesh generation based on node insertion in crystal lattice arrangement and advancing-front-Delaunay triangulation, *Comput. Methods Appl. Mech. Engrg.* **187**, 543–569, (2000).
31. N. Molino, R. Bridson, J. Teran and R. Fedkiw, A crystalline, red green strategy for meshing highly deformable objects with tetrahedra, In *Proceedings of the 12th International Meshing Roundtable*, pp. 103–114, (2003).
32. D. Eppstein, J.M. Sullivan and A. Üngör, Tiling space and slabs with acute tetrahedra, *Computational Geometry: Theory and Applications* **27**, 237–255, (2004).
33. J. Kasper, P. Hagenmuller, M. Pouchard and C. Cros, Clathrate structure of silicon Na_8Si_{46} and $Na_xSi_{136}(x < 11)$, *Science* **150**, 1713–1714, (1965).
34. P. J. Frey, About surface remeshing, In *Proceedings of the 9th International Meshing Roundtable*, pp. 123–156, (2000).
35. D. Wang, O. Hassan, K. Morgan and N.P. Weatherill, Surface grid generation based on remeshing, (preprint).
36. Q. Du and D. Wang, Optimal 3D tetrahedral meshing based on the optimal CVT, (preprint).
37. X.Y. Li, Sliver-free three dimensional Delaunay mesh generation, Ph.D. Thesis, University of Illinois at Urbana-Champaign, (2000).